Available online at www.sciencedirect.com
ScienceDirect
Journal of Molecular Spectroscopy 240 (2006) 174–187
Journal of MOLECULAR SPECTROSCOPY
www.elsevier.com/locate/jms

Rotational energy cluster formation in XY_3 molecules: Excited vibrational states of BiH_3 and SbH_3

Sergei N. Yurchenko [a,*], Walter Thiel [a], Per Jensen [b]

[a] *Max-Planck-Institut für Kohlenforschung, Kaiser-Wilhelm-Platz 1, D-45470 Mülheim an der Ruhr, Germany*
[b] *FB C—Mathematik und Naturwissenschaften, Fachgruppe Chemie, Bergische Universität Wuppertal, D-42097 Wuppertal, Germany*

Received 19 June 2006
Available online 13 October 2006

Abstract

Previous theoretical work on energy cluster formation at high rotational excitation in the vibrational ground state of PH_3 [S.N. Yurchenko, W. Thiel, S. Patchkovskii, P. Jensen, Phys. Chem. Chem. Phys. 7 (2005) 573] is extended to BiH_3 and SbH_3. By means of variational calculations of the rotation–vibration energies based on *ab initio* potential energy surfaces, we analyze the rotational energy clustering of BiH_3 and SbH_3 at $J \leqslant 70$ for a number of vibrational states. We show that BiH_3 and SbH_3, with their pronounced local mode behaviour, exhibit cluster formation already at moderate rotational excitation. In addition, owing to its quasi-spherical-top character, BiH_3 undergoes an imperfect bifurcation at high J. This gives rise to an energy cluster type not present in PH_3 and SbH_3. We present a semi-classical approach to the construction of the rotational energy surfaces for vibrationally excited states.

Keywords: Energy clusters; Rotational energy; Excited vibrational states; Bifurcations; Local mode

1. Introduction

We have recently demonstrated by theoretical calculation [1] that in the vibrational ground state of PH_3, the highly excited rotational states form near-degenerate energy clusters. We have also computed the line strengths for transitions involving these cluster states [2]. In the present work, we study theoretically the energy-cluster formation in BiH_3 and SbH_3. In these molecules, in particular in BiH_3, the energy clusters form at lower rotational excitation than in PH_3 and, in consequence, the theoretical calculation of the cluster energies is computationally less demanding. Because of this, we have been able to extend the study of the cluster phenomenon to the vibrationally excited states of BiH_3 and SbH_3.

The formation of rotational energy clusters in a molecule provides a good example of how a system, which is completely described by quantum mechanics at low energy, approaches the classical limit, at least for the rotational motion, with increasing excitation. The parameter governing the transition is the angular momentum quantum number J (see, for example, Ref. [3]). By studying the rotational motion of the molecule from $J = 0$ to $J \gg 1$, we can follow the continuous change from an entirely quantum mechanical system to one where the rotational motion is classical. This transition connects two modelling paradigms: At the low-energy, quantum-mechanical limit, the molecular rotation is described by a simple rigid-rotor model, whereas at very high energy, another simple model, involving classical trajectories, is applicable. Between the two limits there is an intermediate region with a dense and disordered energy structure which is difficult to interpret.

In highly excited rotational states, we typically find that characteristic 'stable' axes of rotation emerge, about which the molecule prefers to rotate. This type of rotation tends to simplify the rotational energy level pattern since, when several symmetrically equivalent stable axes are present, the rotational energy levels form clusters, that is, groups

* Corresponding author. Fax: +49 208 306 2996.
E-mail address: yurchenko@mpi-muelheim.mpg.de (S.N. Yurchenko).

0022-2852/$ - see front matter © 2006 Elsevier Inc. All rights reserved.
doi:10.1016/j.jms.2006.10.002

of quasi-degenerate energy levels. Dorney and Watson [4] were the first to realize this; they explained the energy cluster formation in spherical top molecules in terms of classical rotation about symmetrically equivalent axes. Subsequently, Harter and co-workers (see, for example, Refs. [5,6]) have developed extensive classical models for the qualitative description of rotational-energy cluster formation in XY_N molecules. They introduced the now well-known concept of a *rotational energy surface* (RES), defined as the classical (or semi-classical) rotational energy of a molecule obtained as a function of the direction (relative to the molecule) of the classical angular momentum vector, which is taken to have a length of $|\mathbf{J}| = \sqrt{J(J+1)}\hbar$. The topology of the RES (in particular its stationary points) defines the patterns of the rotational energy levels. Pavlichenkov and Zhilinskiĭ [7] illustrated how the bifurcation of stationary points on the RES affects the formation of rotational energy clusters. The role of symmetry in the cluster formation process has been also studied in great detail (see, for example, [8]).

In addition to the classical studies there have been many quantitative, quantum-mechanical studies of the rotational cluster formation (see, for example, the reviews [9,10]). This work was concerned with dihydrides H_2X and, to a lesser extent, with methane-type spherical top molecules XY_4. As mentioned above we have recently extended this work to XY_3 molecules in that we have shown by variational, quantum-mechanical calculation that rotational energy clusters form in the vibrational ground state of PH_3. We have characterized two basic types of rotational clusters for PH_3: Two- and sixfold clusters. The twofold clusters are associated with classical rotation about an axis close to the C_3 rotational symmetry axis for a PH_3 molecule at equilibrium; this axis is found to be stable at any value of J. The sixfold energy clusters can be understood as resulting from (clockwise or anti-clockwise) rotation about three symmetrically equivalent axes A (see Fig. 1). These axes lie in planes close to the three planes of reflection of a PH_3 molecule at equilibrium. As J increases, each axis approaches one of the P–H bonds. Thus, in a somewhat simplistic picture, we can think of the rotation in the cluster states at $J \to \infty$ as taking place about the three P–H bonds in PH_3. In this situation, the P–H localized rotation is naturally orthogonal to any other degree of freedom and, thus, reaches the highest degree of separation from these. We know that separations of this kind between vibrational degrees of freedom cause local-mode behaviour [10,11] and it was discussed for triatomic dihydrides H_2X in Ref. [10] how the local mode behaviour is intimately related to the phenomenon of energy clustering. An H_2X molecule whose vibration is well described by a local-mode model will have rotational energy clusters at relatively low rotational excitation. We expect that analogously, XH_3 molecules with pronounced local-mode behaviour will exhibit sixfold energy clusters at relatively low rotational excitation. The PH_3 molecule, however, whose cluster formation has been studied in Refs. [1,2], is far from being an ideal local-mode molecule, and therefore it is not an ideal case for studying cluster formation. The ultimate limit of complete mode separation, achieved by rotational excitation, is physically inaccessible for PH_3: Before it is reached, centrifugal distortion breaks the P–H bonds [1].

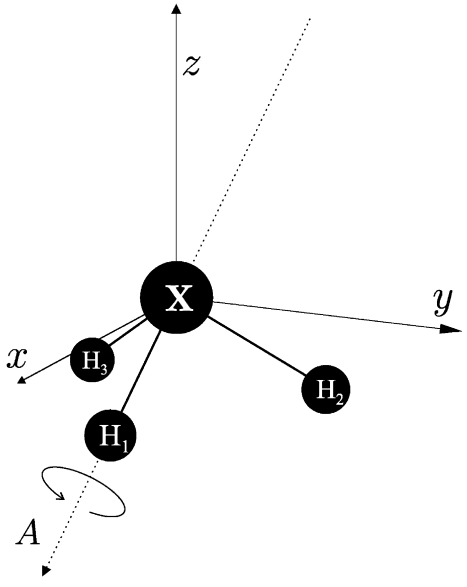

Fig. 1. The labeling of the nuclei chosen for XH_3, the molecule-fixed z axis, and the localization axis A (see text).

In our search for 'ideal' local-mode XY_3 molecules with 'perfect' energy clustering effects, we consider here the molecules BiH_3 and SbH_3. BiH_3 is a typical local-mode molecule [12] with a heavy central Bi atom bound to three much lighter H atoms. It has small intermode coupling and bond angles very close to 90°. The large ratio of the Bi mass to the proton mass, the small intermode coupling, and the near-90° bond angles are all conducive to local mode behaviour [10]. The fact that the Bi–H bonds are almost orthogonal makes them ideally oriented for stable rotations. As mentioned above, for BiH_3 and SbH_3 it is viable to compute highly excited rotational energies in excited vibrational states, and so we can study the cluster formation in these states. Local-mode theory predicts that stretching excitation accelerates the stabilization of the rotational axes [10] and, therefore, it makes the rotational energy clusters form at lower J values than in the vibrational ground state. We show in the present work that the BiH_3 and SbH_3 cluster formation indeed is 'faster' in this sense than that of PH_3. It is even more interesting that the rotational energy level patterns of BiH_3 exhibit special cluster features not found in the case of the less pronounced local-mode molecule PH_3. An important reason for the differences in cluster formation between PH_3 and BiH_3 is that BiH_3 is an almost perfect, accidental spherical top [13]. In order to see how this affects the rotational cluster formation, we compare the results for BiH_3 with those obtained for SbH_3. SbH_3 has local-mode properties very similar to those of BiH_3, but it has a less pronounced spherical top character.

In the present work, we solve variationally the quantum-mechanical Schrödinger equation for the rotation and vibration of the molecules studied to obtain the corresponding energies and wavefunctions. The details of the method used can be found in Refs. [1,14]. For the qualitative description of the cluster formation we also take a classical approach, in which we generate rotational energy surfaces and characterize their stationary points. In order to describe excited vibrational states we employ a 'semi-classical' (or, perhaps more appropriately, 'semi-quantum') analysis, where we use quantum-mechanical techniques to construct an analogue of the classical RES. The classical analysis of the rotational cluster formation in vibrationally excited states was first considered in Refs. [6,15]. The work by van Hecke et al. [16] should also be mentioned as a fairly recent, detailed classical study of the rotational cluster formation in vibrationally excited states of P_4.

The paper is structured as follows. In Section 2, we introduce potential energy surfaces for BiH_3 and SbH_3 together with the analytical representations that we employ. The variational method used for the term value calculations is briefly discussed in Section 3. Rotational term value diagrams for different vibrational states of BiH_3 and SbH_3 are presented and discussed, with special emphasis on the energy cluster formation, in Section 4. In Section 5, we present a classical analysis of the rotational dynamics for BiH_3 based on the RES method. Finally, in Section 6 we offer conclusions.

2. Potential energy surfaces

In order that we can simulate the rotational dynamics of an XH_3 molecule, we need to define its potential energy surface (PES). We employ a Morse-type parameterized potential energy function, expected to provide an accurate description over a broad range of molecular geometries in terms of a small number of parameters (PES type A in Ref. [14])

$$\begin{aligned} V(\xi_1,\xi_2,\xi_3,\xi_{4a},\xi_{4b};\sin\bar{\rho}) &= V_e + V_0(\sin\bar{\rho}) + \sum_j F_j(\sin\bar{\rho})\xi_j + \sum_{j\leqslant k} F_{jk}(\sin\bar{\rho})\xi_j\xi_k \\ &+ \sum_{j\leqslant k\leqslant l} F_{jkl}(\sin\bar{\rho})\xi_j\xi_k\xi_l + \sum_{j\leqslant k\leqslant l\leqslant m} F_{jklm}(\sin\bar{\rho})\xi_j\xi_k\xi_l\xi_m. \end{aligned} \tag{1}$$

This function is expressed in terms of the stretching variables

$$\xi_k = y_k = 1 - \exp[-a(r_k - r_e)], \quad k = 1,2,3, \tag{2}$$

where a is a Morse parameter, the symmetrized bending variables

$$\xi_{4a} = S_{4a} = \frac{1}{\sqrt{6}}(2\alpha_1 - \alpha_2 - \alpha_3), \tag{3}$$

$$\xi_{4b} = S_{4b} = \frac{1}{\sqrt{2}}(\alpha_2 - \alpha_3) \tag{4}$$

and the variable

$$\sin\bar{\rho} = \frac{2}{\sqrt{3}}\sin[(\alpha_1+\alpha_2+\alpha_3)/6] \tag{5}$$

for the 'umbrella' motion. Here, r_i is the instantaneous value of the distance between the central X nucleus (where X is Bi or Sb) and H_i, where H_i is the proton labeled i (= 1, 2, or 3); α_i denotes the bond angle $\angle(H_j XH_k)$, where (i,j,k) is a permutation of the numbers $(1,2,3)$. The quantity r_e is the common equilibrium value of the three distances r_i. The functions $V_0(\sin\bar{\rho})$ and $F_{jk\ldots}(\sin\bar{\rho})$ in Eq. (1) are defined as

$$V_0(\sin\bar{\rho}) = \sum_{s=1}^{4} f_0^{(s)}(\sin\rho_e - \sin\bar{\rho})^s, \tag{6}$$

$$F_{jk\ldots}(\sin\bar{\rho}) = \sum_{s=0}^{N} f_{jk\ldots}^{(s)}(\sin\rho_e - \sin\bar{\rho})^s, \tag{7}$$

where $\sin\rho_e$ is the equilibrium value of $\sin\bar{\rho}$ and the quantities $f_0^{(s)}$ and $f_{jk\ldots}^{(s)}$ in Eqs. (6) and (7) are expansion coefficients. The summation limits in Eq. (7) are $N=3$ for $F_j(\sin\bar{\rho})$, $N=2$ for $F_{jk}(\sin\bar{\rho})$, $N=1$ for $F_{jkl}(\sin\bar{\rho})$, $N=0$ for $F_{jklm}(\sin\bar{\rho})$. In total there are 47 symmetrically unique potential parameters $f_{jk\ldots}^{(s)}$.

The values of the parameters $f_{ij\ldots}^{(s)}$ in Eqs. (6) and (7), that define the analytical PES of BiH_3, are obtained from the high-level *ab initio* potential energy surface P4 reported in Ref. [17]. The P4 PES is given in Ref. [17] as a standard 'force-constant' expansion (truncated after the quartic terms) in internal displacement coordinates $r_i - r_e$ and $\alpha_i - \alpha_e$ ($i = 1$, 2, or 3), where α_e is the common equilibrium value of the three α_i. We determine the values of the coefficients $f_{ij\ldots}^{(s)}$ in Eqs. (6) and (7) by analytical transformation of the P4 PES. Towards this end, we generate Taylor expansions of the internal coordinates r_i and α_i ($i = 1,2,3$) in terms of the variables ξ_j ($j = 1,2,3,4a,4b$) and $\sin\rho_e - \sin\bar{\rho}$, and we insert these Taylor expansions in the P4 function. In the work on SbH_3 reported below, we employ a PES obtained in an analogous manner from the force constants given in Ref. [18]. For both BiH_3 and SbH_3, the Morse parameter a has been adjusted to produce an analytical PES, given by Eq. (1), that reproduces as well as possible the original force-constant expansions [17,18] truncated after second order. The equilibrium parameter ρ_e is given in terms of the equilibrium bond angle α_e

$$\rho_e = \pi - \arcsin\left[\frac{2}{\sqrt{3}}\sin\frac{\alpha_e}{2}\right]. \tag{8}$$

We list the determined values of the parameters $f_{jk\ldots}^{(s)}$, a, r_e, and α_e in Table 1. In order to investigate the quality of the corresponding analytical PES's, we variationally calculate the vibrational term values for SbH_3 and BiH_3, using the parameter values in Table 1 as input. The results are presented in Table 2, where we compare them to the available experimental data. In the present

Table 1
Potential energy parameters[a] (in cm^{-1} unless otherwise indicated) for the electronic ground states of BiH_3 and SbH_3

Parameter	SbH_3	BiH_3
α_e/deg[b]	91.56	90.32
r_e/Å[b]	1.70001	1.77834
a/Å^{-1}	1.40	1.39
f_0^2	269405.57	239198.30
f_0^3	−649168.93	−563131.75
f_0^4	2061132.21	1853073.22
f_1^1	−9028.96	−5631.20
f_1^2	−14578.68	−26820.53
f_1^3	−60823.94	3529.62
f_{11}^0	29495.17	25497.17
f_{11}^1	−143.23	1851.26
f_{11}^2	−45323.31	−50721.08
f_{12}^0	−125.68	−112.04
f_{12}^1	8919.27	9222.87
f_{12}^2	−16778.55	−14420.65
f_{14}^0	−852.00	−552.96
f_{14}^1	−18374.76	−17449.72
f_{14}^2	−23586.82	−19734.08
f_{44}^0	15449.71	14120.47
f_{44}^1	40167.63	38787.43
f_{44}^2	−27953.96	−9828.90
f_{111}^0	−628.58	−344.99
f_{111}^1	1423.76	1181.10
f_{112}^0	−205.28	−29.93
f_{112}^1	2657.88	601.43
f_{114}^0	284.72	436.76
f_{114}^1	−19309.12	−19163.77
f_{123}^0	−178.02	−91.37
f_{123}^1	3106.59	707.57
f_{124}^0	1455.91	1418.35
f_{124}^1	5434.55	5422.32
f_{144}^0	−1777.50	−1670.09
f_{144}^1	−7851.91	−8647.05
f_{155}^0	−4786.81	−4529.54
f_{155}^1	−9114.78	−12169.70
f_{455}^0	−6471.25	−6803.50
f_{455}^1	−59547.70	−61254.58
f_{1111}^0	1338.38	1170.93
f_{1112}^0	−96.07	73.46
f_{1114}^0	330.41	108.45
f_{1122}^0	188.31	386.11
f_{1123}^0	−130.86	−104.45
f_{1124}^0	203.69	−66.26
f_{1125}^0	260.17	−119.89
f_{1144}^0	−1720.44	−1524.71
f_{1155}^0	−4900.62	−4727.73
f_{1244}^0	836.25	811.35
f_{1255}^0	1603.72	1442.39
f_{1444}^0	−869.92	−915.85
f_{1455}^0	652.48	519.92
f_{4444}^0	2537.99	2712.09

[a] Only symmetrically unique parameters are given.
[b] Experimental values from Refs. [18] (SbH_3) and [19] (BiH_3).

study, we do not aim for an extremely high numerical accuracy; the purpose of the work is a more qualitative analysis of the energy level patterns resulting from the cluster formation. In view of this, we find the agreement between theory and experiment in Table 2 to be satisfactory.

3. Variational calculations

We calculate rovibrational energies of BiH_3 and SbH_3 by means of a variational approach described in detail in Ref. [14]. This approach is designed for the simulation of rotation–vibration spectra of XY_3 pyramidal molecules (for the calculation of intensities, see Refs. [21,22]). The approach is based on the Hougen–Bunker–Johns formalism [23] and applicable to isolated electronic states of any pyramidal XY_3 molecule. The vibrational motion is viewed as producing displacements from a flexible *reference configuration* defined by Eckart–Sayvetz conditions [24,25]. The reference configuration follows the 'umbrella' motion of the molecule, it has $\mathscr{C}_{3v}$ geometrical symmetry and the molecule-fixed axis system [3] is attached to it. In the Hougen–Bunker–Johns approach, the rotation–vibration coordinates are chosen to provide maximum separation between the different types of molecular motion: Rotation, umbrella motion, and the other vibrations. The molecule-fixed z axis is a C_3 rotational symmetry axis of the molecule at the reference configuration. The x-axis is defined so that the xz plane contains the X nucleus (Bi or Sb) and the proton H_1 with the x coordinate of H_1 being positive. The coordinate system is shown in Fig. 1.

We do not give any technical details of the variational calculation here; these details can be found in Ref. [14]. Suffice it to say that we diagonalize a matrix representation of the rotation–vibration Hamiltonian set up in a suitable basis set. The basis functions are labeled by the principal quantum numbers (v_1, v_2, v_3, v_4), where v_1 and v_3 are associated with the stretching basis functions, v_2 describes the 'umbrella' excitation, and v_4 describes the excitation of the small-amplitude bending mode. The basis set is truncated according to

$$P = 2(v_1 + v_3) + v_2 + v_4 \leqslant P_{\max}. \tag{9}$$

We use the value $P_{\max} = 6$ for the semi-quantitative analysis of rovibrational spectra at high J (here, J up to 70). The basis set truncation errors are found to be about 0.03 cm^{-1} for the vibrational ground state and 0.25, 0.4, 1, and 10 cm^{-1} for the v_2/v_4, v_1/v_3, $2v_2/v_2 + v_4/2v_4$, and $2v_1/(v_1 + v_3)/2v_3$ vibrational manifolds, respectively. The effect of the basis set extension appears to be a systematic, simultaneous lowering of all energies, so that all 'local' energy distributions remain qualitatively unchanged as the basis set is enlarged.

The kinetic energy operator, given by the factor $G_{\lambda\mu}$, and the pseudo-potential function U are truncated after the 4th order of the expansion [14]. The potential energy function Eq. (1) is transformed into a 6th order expansion (PES type B in Ref. [14]) in terms of the linearized coordinates that are used to describe the vibrational motion in the approach of Ref. [14].

Table 2
Variationally calculated term values (in cm^{-1}) of BiH_3 and SbH_3, compared to the available experimental data [12,19,20]

State	SbH_3			BiH_3		
	Obs.	Calc.	Obs. − Calc.	Obs.	Calc.	Obs. − Calc.
v_2	782.13	798.90	−16.77	726.70	733.91	−7.21
v_4	827.83	836.84	−9.01	751.24	759.52	−8.28
v_1	1890.40	1893.82	−3.42	1733.25	1742.40	−9.14
v_3	1894.38	1899.14	−4.76	1734.47	1746.29	−11.82
$v_1 + v_3$	3719.64	3730.59	−10.95	3406.36	3428.31	−21.95
$2v_1$	3719.71	3730.60	−10.89	3406.70	3428.43	−21.73
$3v_3$	5479.93	5500.49	−20.56			
$3v_1$	5479.93	5500.60	−20.67			
$2v_1 + 2v_3$	7173.37	7209.74	−36.37			
$4v_1$	7173.39	7209.75	−36.36			

4. Rotation–vibration energies. A quantum-mechanical study of the rotational cluster formation

4.1. The vibrational ground state

We have computed rovibrational term values of BiH_3 and SbH_3 for $J \leqslant 70$. As mentioned above, the present study is semi-quantitative only and so, throughout the paper we prefer to present the results in diagrams rather than in tables. We denote a calculated term value by $E_{v,Jk}$, where v is a short-hand notation for the vibrational quantum numbers (v_1, v_2, v_3, v_4) with $v = 0$ identifying the vibrational ground state, and k is the projection of the angular momentum onto the molecular z axis (see, for example, Ref. [3]). In order to visualize the cluster formation, we plot rotational term value spacings $E_{v,Jk} - E^{\max}_{v=0,J}$ against J, where $E^{\max}_{v=0,J}$ is the maximum energy in a given J multiplet of the $v = 0$ state. Term value diagrams of this type for the vibrational ground states of BiH_3 and SbH_3 are given in Fig. 2. In the figure, we indicate for each energy level its value of $(K_{\rm lc}/J) \leqslant 1$, where $K_{\rm lc} \geqslant 0$ ('lc' stands for 'largest contribution') is the K-value ($K = |k|$) of the basis function with the largest contribution to the eigenfunction of the state in question; the determination and significance of $K_{\rm lc}$ are discussed in detail below.

In the vibrational ground states of BiH_3 and SbH_3, the rotational energies at the top of the J manifolds form clusters of four distinct energies. In Fig. 2, we identify these clusters by circles; a cluster is indicated when the four term values in it lie within a 0.1-cm^{-1} interval. The states in a cluster span the reducible representation

$$\Gamma_{\rm Cluster} = A_1 \oplus A_2 \oplus 2E \tag{10}$$

of the Molecular Symmetry Group $\mathscr{C}_{3v}$(M) [3]. The states of highest and lowest energy in each cluster span the representation $A_1 \oplus A_2$;[1] the two 'inner' E states are sandwiched between these 'outer' states. Since the E irreducible representation is doubly degenerate, each cluster comprises six rotation–vibration states. The energy clusters are readily

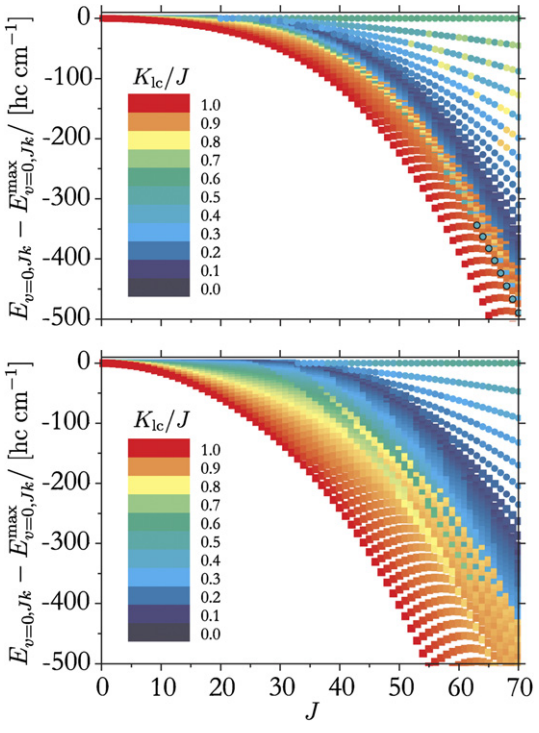

Fig. 2. Rotational term value spacings $E_{v=0,Jk} - E^{\max}_{v=0,J}$ for the vibrational ground states of BiH_3 (top) and SbH_3 (bottom). For each energy level, the value of $K_{\rm lc}/J$ is indicated; $K_{\rm lc}$ is the K-value of the basis function with the largest contribution to the eigenfunction of the state in question (see text).

recognized in Fig. 3 where we enlarge the top parts of the two displays in Fig. 2. The clusters are analogous to those described for PH_3 in Ref. [1] but, in particular in BiH_3, they form at significantly lower J values than in PH_3. As mentioned above, in the semi-classical limit the states in a sixfold cluster correspond to six equivalent stable rotations about three symmetrically equivalent axes A. For each axis, clockwise and anti-clockwise rotation can take place so that the three axes give rise to a total of six equivalent states. At $J \to \infty$ each axis tends to coincide with an X–H_i bond [1].

Fig. 4 shows the *cluster spread* (i.e., the difference between the highest and lowest term values of the sixfold cluster) for the 'top' clusters (the clusters at highest energy

[1] Where, for J even, the state at highest energy has A_1 symmetry and that at lowest energy A_2 symmetry. For J odd it is the other way around.

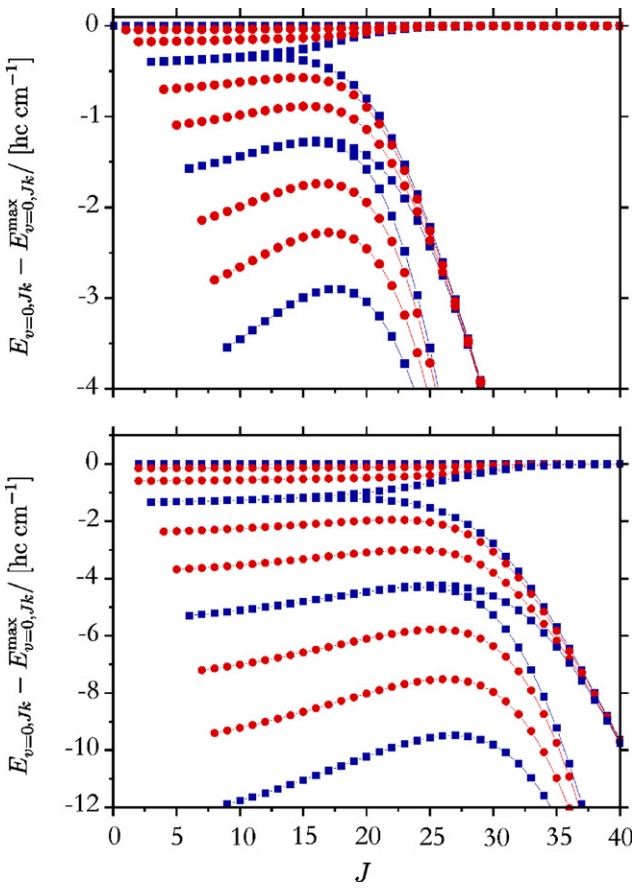

Fig. 3. Rotational term value spacings $E_{v=0,Jk} - E^{max}_{v=0,J}$ for the highest rotational energies in the vibrational ground states of BiH_3 (top) and SbH_3 (bottom). Squares indicate levels of A_1 or A_2 symmetry in $\mathscr{C}_{3v}$(M) [3]; circles indicate levels of E symmetry.

in the J manifold) for various vibrational states of BiH_3 and SbH_3. A detailed analysis of the data in the figure shows that at high J, the cluster spread decreases exponentially with J for both molecules as already discussed for PH_3 in Ref. [1]. The exponential decrease has been explained by Harter and Patterson [5] in terms of RES theory. In BiH_3, the clusters obviously form at lower J than in SbH_3 (note the different ordinate scales in the two displays of Fig. 4). This is not simply a consequence of the Bi nucleus being heavier than the Sb nucleus. Instead, it is caused by the fact that BiH_3 is a near-spherical top. For a 'true,' rigid spherical top, all energies in a given J manifold are degenerate. Thus, the energies in the J manifolds of BiH_3 are very closely spaced, and relatively little centrifugal distortion is required to bring about the cluster formation. For a given J value, the energies in the corresponding J manifold in the vibrational ground state of SbH_3 lie in an energy interval typically about twice as large as that containing the energies in the same J manifold of BiH_3. However at high J values, the SbH_3 cluster spreads are comparable to those of BiH_3. The strong centrifugal forces associated with the high rotational excitation destroy the spherical-top character of BiH_3 so that its rotational motion becomes similar to that of SbH_3.

If BiH_3 and SbH_3 were rigid molecules, the K_{lc}-values indicated in Fig. 2 would be equal to K_c, the absolute value of the projection, in units of $\hbar$, of the angular momentum onto the z axis (equal to the c principal axis [3]) for a rigid, oblate symmetric rotor. In the rigid-rotor case the lowest energy in each J manifold would have $K_c = J$ and, as the energies within the manifold increase, K_c would decrease so that the highest energy has $K_c = 0$. We consider here a vibrating molecule for which K_c is no longer a good quantum number. The 'effective' K-labeling in Fig. 2 is obtained by considering the rotation–vibration wavefunctions $\psi_n^{J,\Gamma}$ for the states in question. In our model, these wavefunctions are given as linear combinations of the basis functions $\phi_{v,K}^{J,m}$

$$\psi_n^{J,\Gamma}(r_1, r_2, r_3, \alpha_1, \alpha_2, \alpha_3, \theta, \phi, \chi) = \sum_{K=0}^{J} \sum_{v} C_{v,K}^{n,J,\Gamma} \phi_{v,K}^{J,m}, \qquad (11)$$

where the $C_{v,K}^{n,J,\Gamma}$ are expansion coefficients, v is again a short-hand notation for the vibrational quantum numbers (v_1, v_2, v_3, v_4), Γ is the $\mathscr{C}_{3v}$(M) symmetry of $\psi_n^{J,\Gamma}$, and n is a running index used to distinguish eigenfunctions with the same values of J and Γ. The K-value K_{lc} given in Fig. 2 is that for which $|C_{v,K}^{n,J,\Gamma}|^2$ is largest in Eq. (11). That is, it is the K-value of the basis function $\phi_{v,K}^{J,m}$ with the largest contribution to the eigenfunction $\psi_n^{J,\Gamma}$.

The distribution of K_{lc}-values shown in Fig. 2 is found to be very different from that predicted in the rigid-rotor

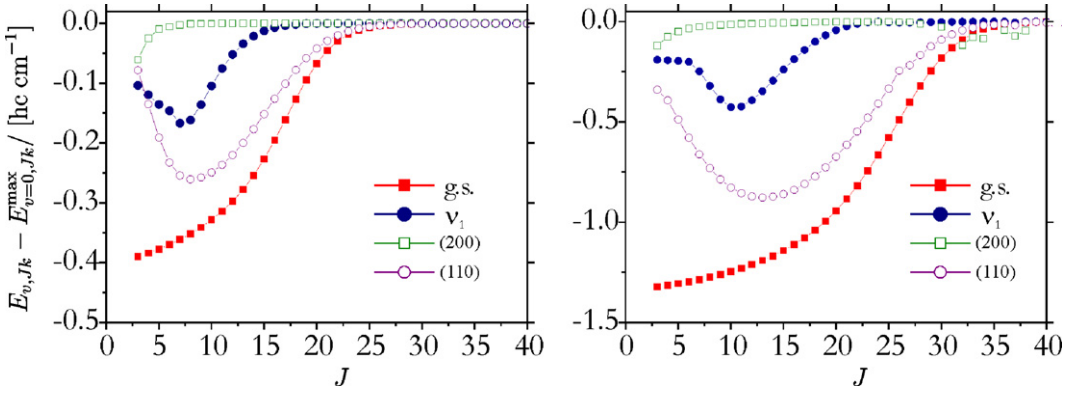

Fig. 4. Cluster spreads (see text) for BiH_3 (left) and SbH_3 (right).

model. For both BiH_3 and SbH_3, the lowest energies in the J manifolds have $K_{lc} = K_c = J$ as expected, and as the energies within the manifold increase, K_{lc} decreases. However, K_{lc} reaches values near zero before we arrive at the highest energy with the given value of J; there is a region with $K_{lc} \approx 0$ in the middle of the manifolds. For the states with term values above this region, K_{lc} has intermediate values between, say, $0.5J$ and $0.8J$. These states are the sixfold cluster states; they are indicated by circles in Fig. 2. The states with $K_{lc} = J$ at the bottom of the J manifolds correspond to twofold clusters ($k_c = \pm K_c = \pm J$; see Ref. [3]) associated with rotation about the z (or C_3) axis. In the following, we refer to the twofold clusters below the $K_{lc} = 0$ 'separation' region as Type A clusters, whereas the sixfold clusters above the separation region are called Type B clusters.

For BiH_3 only, we find in Fig. 2 a progression of sixfold clusters with $J > 60$ situated below the $K_{lc} = 0$ 'separation' region. These cluster states have $K_{lc}/J \approx 0.4$, whereas the states surrounding them in the diagram have $K_{lc}/J \approx 0.9$. Analogous clusters have not been found for PH_3 in the theoretical study of Ref. [1]. We refer to these 'new' BiH_3 clusters as Type C clusters. The cluster states span the $\mathscr{C}_{3v}(M)$ representation given in Eq. (10), that is, also Type C clusters are formed by two E-symmetry levels approaching an A_1/A_2 level pair. A detailed analysis of the formation of these clusters show that they emerge by coalescence of three twofold clusters. In the following section, we analyse the Type C clusters in terms of RES theory [5]. As usual, the n-fold cluster states are related to n stable rotational axes A corresponding to n stationary points on the RES.

4.2. Excited vibrational states

Term value diagrams with the rotational energy structure in excited vibrational states v_2/v_4, v_1/v_3, $2v_1/2v_3/(v_1 + v_3)$ and $2v_2/(v_2 + v_4)/2v_4$ are shown in Fig. 5 for BiH_3 and in Fig. 6 for SbH_3. In both figures, sixfold clusters are represented by filled circles. We indicate clusters whose cluster spreads are 0.1 cm^{-1} or less. The term value diagrams for SbH_3 in Fig. 6 are obviously rather similar to those for BiH_3 in Fig. 5 (with the sixfold energy clusters forming at lower J-values in BiH_3). In view of this similarity, we concentrate on BiH_3 in the discussion of the cluster structure.

4.2.1. Bending excitation: The v_2/v_4 and $2v_2/(v_2 + v_4)/2v_4$ polyads

In BiH_3, the experimentally determined vibrational term values for the v_2 and v_4 fundamental levels are 726.7 and 751.2 cm^{-1}, respectively. The v_2 normal mode has A_1 symmetry in $\mathscr{C}_{3v}(M)$, whereas v_4 has E symmetry. In the v_2/v_4 display of Fig. 5, at very low J the term values group into a v_2 component at low energy and a v_4 component at higher energy. Since the v_4 state is degenerate, Coriolis coupling effects cause the v_4 component to split into two sub-components at $J > 5$, this is similar to the splittings of the E-state energy distributions seen in theoretical calculations for SiH_4 and CH_4 [26]. It is interesting that at J values above 30 the entire v_2/v_4 system coalesces into one component; there is no longer any clear distinction between the v_2 manifold and the two Coriolis-split components of the v_4 manifold. This is analogous to the findings of Kozin and Jensen for the v_1/v_3 manifolds of H_2Se [27] and other dihydrides H_2X [9]:

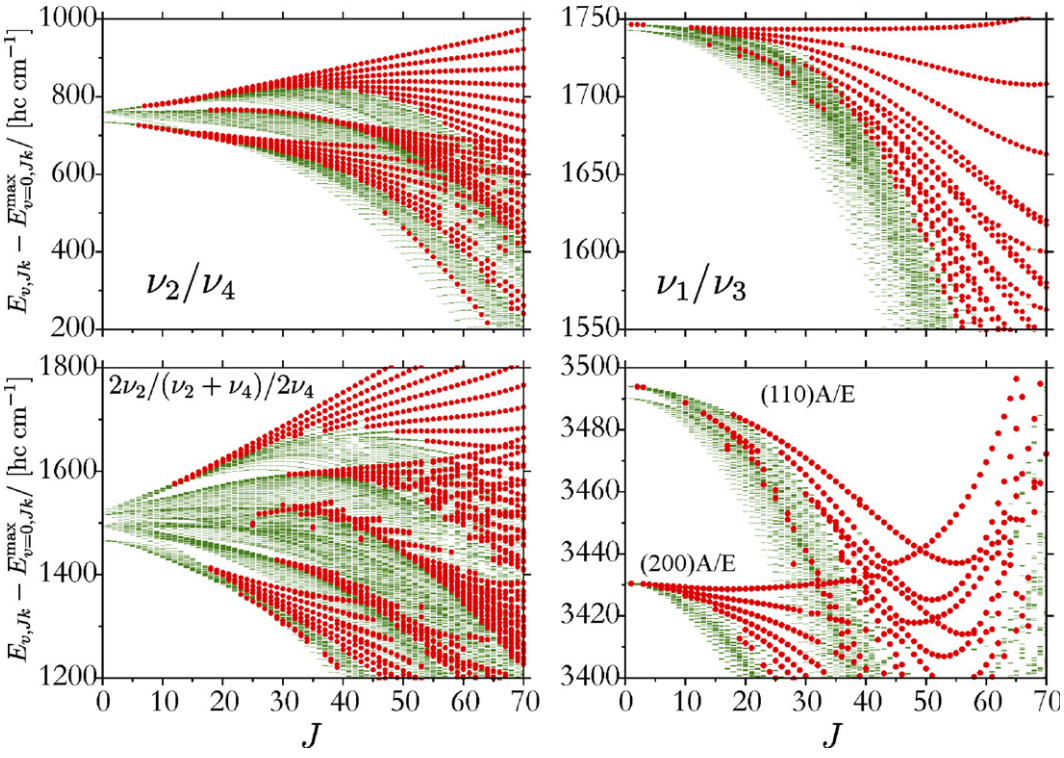

Fig. 5. Rotational energy levels for BiH_3 in excited vibrational states. For notation, see Fig. 2.

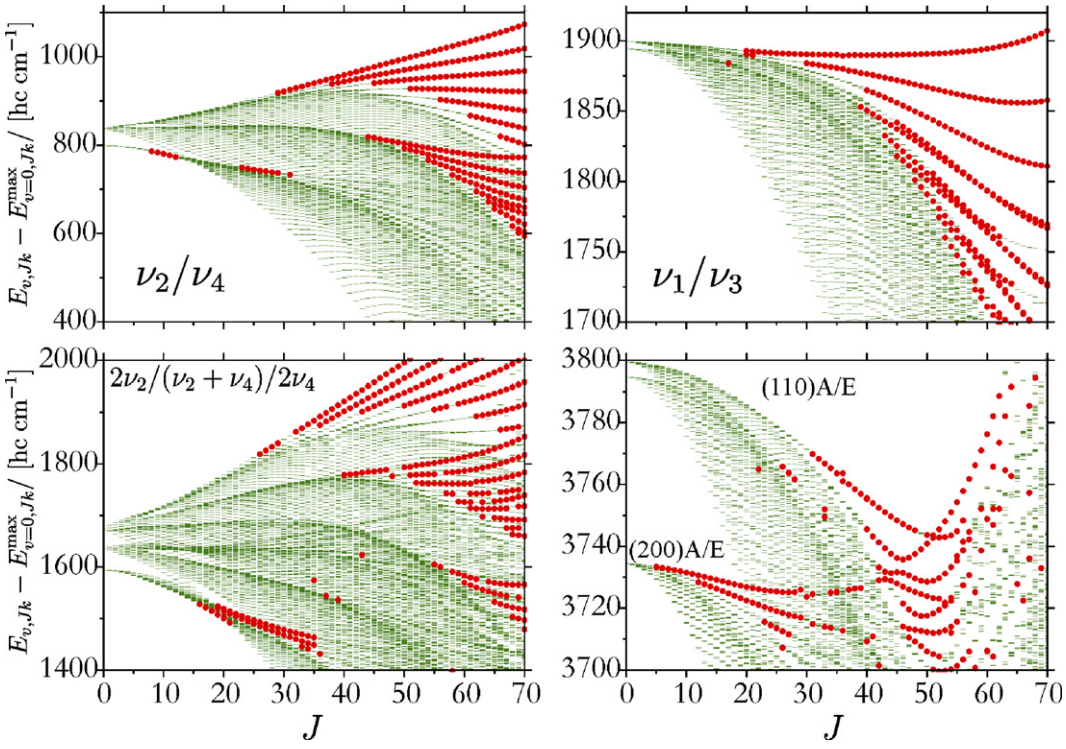

Fig. 6. Rotational energy levels for SbH_3 in excited vibrational states. For notation, see Fig. 2.

Rotational excitation removes the distinction between the normal-mode vibrational states and induces local-mode behaviour. Fig. 5 shows that also for BiH_3, the local-mode labeling scheme is appropriate at high J. All three vibrational components in the ν_2/ν_4 display of Fig. 5 develop rotational energy clusters as J increases. The clusters in the central vibrational component (i.e., the lower Coriolis-split component of the ν_4 state) appear at higher J values ($J \approx 50$) than in the other two components.

At very high J, each J manifold of the ν_2/ν_4 dyad contains very many states, the density of states is thus high and there is ample opportunity for (avoided) crossings and interactions. Although the resulting patterns are highly disordered, in most cases it is still possible to recognize the cluster features. The states with lowest energy in the J manifolds form twofold clusters (Type A), there is an intermediate, irregular region, and above this region the sixfold clusters of Type B form. A few Type C clusters have been identified among the ν_2 energies at $J \approx 55$.

The energy level structure of the polyad $2\nu_2/(\nu_2+\nu_4)/2\nu_4$ of doubly excited bending states is qualitatively similar to that of the dyad ν_2/ν_4. The term values now group into six sub-components and very many clusters form at high J. However, there is again a high density of states and many more or less accidental interactions. Consequently, only at the top of the J manifolds for the entire polyad are there unperturbed progressions of sixfold clusters. Rotational excitation removes the distinction between the rotational structures of the individual normal-mode vibrational states also in the case of $2\nu_2/(\nu_2+\nu_4)/2\nu_4$ polyad.

4.2.2. Stretching excitation: The ν_1/ν_3 and $2\nu_1/2\nu_3/(\nu_1+\nu_3)$ polyads

We now consider the stretching fundamental levels ν_1 (A_1 symmetry in $\mathscr{C}_{3v}$(M)) and ν_3 (E symmetry) together with the polyad $2\nu_1/2\nu_3/(\nu_1+\nu_3)$ of overtone and combination levels, for BiH_3 and SbH_3. We label the overtone and combination levels by local-mode quantum numbers ($lmn\Gamma_{vib}$), where l, m, and n are the number of excited quanta in each of the three bond oscillators (see, for example, Ref. [12]), while Γ_{vib} is the vibrational symmetry in $\mathscr{C}_{3v}$(M) [3]. The three overtone and combination levels considered here, $2\nu_1$, $\nu_1+\nu_3$, and $2\nu_3$, have the local-mode labels ($200A$), ($200E$), and ($110A/E$), respectively.

The rotational energy level pattern in the ν_1/ν_3 polyad of BiH_3 (Fig. 5) is dominated by the pronounced local mode character of this polyad: The ν_1 and ν_3 states are nearly degenerate. This leads to the formation of sixfold clusters analogous to the Type II clusters found for triatomic molecules (see Ref. [10] and references therein). These clusters appear at low J and involve heavy mixing of the ν_1 and ν_3 vibrational basis functions. In the $2\nu_1/2\nu_3/(\nu_1+\nu_3)$ polyad, matters are complicated by local interactions leading to avoided crossings of cluster-state progressions. These avoided crossings are generally between progressions of, on one hand, ($200A$) and ($110A$) cluster states and, on the other hand, ($200E$) and ($110E$) cluster states. Cluster state progressions originating in A vibrational states generally just cross the progressions originating in E vibrational states. In the avoided crossings, at least on the scale of Fig. 5, the six near-degenerate cluster states appear as

one state, each member of a cluster interacting to the same extent with a partner member of the same symmetry in the other cluster. This effect has already been noted for triatomic molecules [9,27].

We know that local mode behaviour is conducive to energy cluster formation (see, for example, Ref. [10]), and we also know that excited stretching vibrational states with the entire excitation in a single bond, such as $(200A/E)$, show more pronounced local mode behaviour than the states $(110A/E)$. Hence it is not surprising that in the $(200A)$ and $(200E)$ states (which correlate with the $2v_1$ and v_1+v_3 states, respectively), sixfold clusters form for BiH_3 and SbH_3 at J values lower than those found for the vibrational ground states, as seen from the cluster spreads of Fig. 4. In the $(200A)$ (or $2v_1$) state, the cluster formation is extremely rapid.

5. Classical analysis

In the present section, we discuss the mechanisms leading to the energy cluster formation in terms of classical concepts, most notably in terms of the rotational energy surface [5,6]. We make this analysis for BiH_3 only. The analysis for SbH_3 is essentially a repetition of the classical analysis of the cluster formation in PH_3 reported in Ref. [1]. For BiH_3, however, there are new aspects of the analysis in that we use the classical theory to explain the Type C clusters not found for PH_3 and SbH_3.

5.1. The rotational energy surface

As mentioned in Section 1, Harter and Patterson [5,6] have shown how, by analysing the topology of the rotational energy surface (or RES), we can explain and predict energy cluster formation. To obtain the RES, we must express the classical rotational energy of the molecule in terms of the orientation of the classical angular momentum vector **J** relative to the molecule. This orientation is conveniently described by a polar angle θ and an azimuthal angle ϕ defined in terms of the molecule-fixed axis system xyz [3]. In the customary manner, $\theta \in [0,\pi]$ is the angle between **J** and the molecule-fixed z axis, and $\phi \in [0,2\pi]$ is the angle between the x axis the projection of **J** in the xy plane, measured in the usual positive sense (see, for example, Ref. [3]). The molecular rotation can be understood by analysing the classical trajectories traced by the tip of the vector **J**. The stationary points of the classically defined RES can be used to characterize the cluster phenomena in the quantum-mechanical description: If the RES has n symmetrically equivalent stationary points, there will be n-fold degenerate energy clusters [5]. The cluster states correlate with the smallest possible, classically allowed trajectories of **J** around the n stationary points.

Classical trajectories are defined as solutions of the equations of motion for the classical rovibrational Hamiltonian $H_{\rm rv}$ with the xyz components of the quantum-mechanical angular momentum operator **J** substituted by their classical analogues

$$J_x = \sqrt{J(J+1)}\sin\theta\cos\phi \tag{12}$$

$$J_y = \sqrt{J(J+1)}\sin\theta\sin\phi \tag{13}$$

$$J_z = \sqrt{J(J+1)}\cos\theta, \tag{14}$$

and the generalized momenta $p_n = \partial T/\partial\dot{q}_n$ set to zero [28]. Here T is the classical kinetic energy and the momentum p_n, $n = 1,2,\ldots,6$, is conjugate to the generalized coordinate $q_n \in \{r_1, r_2, r_3, \alpha_1, \alpha_2, \alpha_3\}$. The classical Hamiltonian $H_{\rm rv}$ is defined in terms of the same kinetic-energy expansion coefficients $G_{\lambda\mu}$, the pseudo-potential U, and the potential energy V [14] that we use for the quantum-mechanical, variational calculations presented above.

In practice, we construct the rotational energy surface $E_J(\theta,\phi)$ as follows. We choose a regular grid of angle points θ_m, ϕ_m and optimize the molecular structure (defined by the geometrical parameters r_i and α_i, see above) at each grid point by minimizing the classical energy $E = H_{\rm rv}(r_i,\ \alpha_i,\ \theta_m,\ \phi_m)$. The rotational energy surface $E_J(\theta_m,\phi_m)$ is then given by

$$E_J(\theta_m,\phi_m) = H_{\rm rv}(J, r_i = r_i^{\rm opt}, \alpha_i = \alpha_i^{\rm opt}, \theta_m, \phi_m), \tag{15}$$

where the classical Hamiltonian function $H_{\rm rv}$ is calculated at the optimized geometries $r_i^{\rm opt}, \alpha_i^{\rm opt}$ for each orientation of the angular momentum defined by the polar and azimuthal angles (θ_m, ϕ_m). The RES $E_J(\theta_m, \phi_m)$ is constructed in such a manner that the vibrational motion, or at least the way that the vibration is influenced by centrifugal forces, is incorporated to some extent.

In Fig. 7, we show the RES obtained for BiH_3 at $J = 60$. The stationary points on the RES define stable rotational axes A—we also speak about *local rotational equilibria* in this situation. The RES in Fig. 7 has six distinct equivalent maxima corresponding to local rotational equilibria. The six maxima can be organized in three pairs where the two members of each pair describe clockwise and anti-clockwise rotation, respectively, about the same rotational axis, and so the six maxima define three stable rotational axes only. We always find one stable axis in the plane with $\phi = 0°$ (it has $\theta > 90°$ so that it 'points downwards'), and we can obtain the two other stable axes by letting the $\mathscr{C}_{3v}$

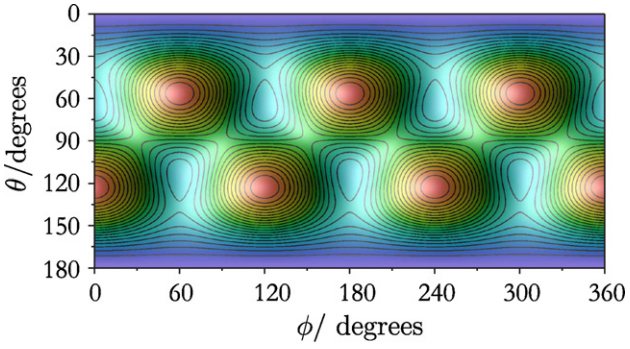

Fig. 7. Rotational energy surfaces for BiH_3 calculated for $J = 60$.

point group operations C_3 and C_3^2 [3] act on this initial axis; they have the same value of θ as the initial axis, but $\phi = 120°$ and 240°, respectively. At $J = 60$, the initial stable axis for BiH_3 with $\phi = 0°$ has $\theta = 122.9°$ (see Fig. 7).

We have analyzed RES's of BiH_3 for J up to 120. The six maxima discussed above appear at any value of $J > 0$. Even at low rotational excitation, centrifugal distortion breaks the $\mathscr{C}_{3v}$ geometrical symmetry of the molecule and the three equivalent rotation axes emerge. As found for PH_3 [1], however, the average molecular geometry associated with rotation about the stable axes has $\mathscr{C}_s$ geometrical symmetry: The two bonds, which are not near the stable rotation axis, are equally stretched. At very high J (>60), the stationary axes tend to coincide with one of the Bi–H bonds, with the two other bonds being almost perfectly orthogonal to this bond and to each other. As J increases, centrifugal distortion keeps elongating the two bonds orthogonal to the rotation axis until they break at $J > 120$.

In addition to the six equivalent maxima just discussed, we find on the RES for any J-value two minima with $\theta = 0°$ and 180°, respectively. That is, the RES has a minimum when the **J** vector points in the positive or negative z direction. These minima correspond to rotations about the z-axis with the $\mathscr{C}_{3v}$ geometrical symmetry conserved. The six maxima and two minima have already been reported in our analysis of the energy cluster formation in PH_3 [1]. However, on the RES of BiH_3 (Fig. 7) we can identify six further minima which were not found in case of PH_3 [1]. These six local rotational equilibria define three additional stable rotational axes that lie in the $\mathscr{C}_{3v}$ planes of reflection. For $J = 60$ one of the additional axes is found at $\theta = 65.6°$, $\phi = 0°$ (i.e., it 'points upwards') and we obtain the two other axes by letting C_3 and C_3^2 [3] act on the first one. The corresponding optimized molecular structure has $\mathscr{C}_s$ geometrical symmetry with α_1=95.8°, α_2=α_3=85.6°, $r_1 = 1.81$ Å, and $r_2 = r_3 = 1.82$ Å. In total, we have found $6 + 6 + 2 = 14$ rotational equilibria for BiH_3, this number is in accordance with the predictions of Ref. [29].

We can appreciate from the discussion of Fig. 7 that all important features of the RES are found in the planes with $\phi = 0°$, 120°, and 240°, respectively. Furthermore, the features at $\phi = 120°$ and 240° are 'repetitions' of those at $\phi = 0°$, obtained by applying the point group operations C_3 and C_3^2 [3] to the $\phi = 0°$ plane. All RES points with $\phi = 0°$ have zero ϕ-gradients

$$\left.\frac{\partial E_J}{\partial \phi}\right|_{\theta,\phi=0} = 0. \tag{16}$$

For $\phi = 0°$, we have minima at $\theta = 0$ and 180°, respectively, one of the six equivalent maxima at $\theta > 90°$, and one of the six equivalent minima at $\theta < 90°$. Owing to the C_3 rotational symmetry of the RES, we can obviously focus on the plane with $\phi = 0°$ in the analysis. In Fig. 8, we show one-dimensional cuts through the RES of BiH_3 with $\phi = 0°$ and $J = 20$, 40, 60, 80, 100, and 120. At $J > 120$ the classical analysis is no longer possible; the molecule has

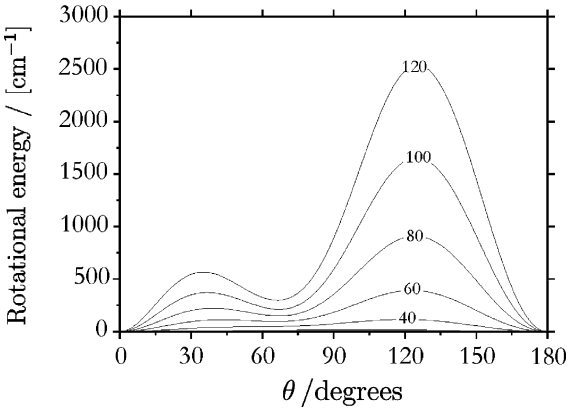

Fig. 8. One-dimensional cuts (for $\phi = 0°$) through the rotational energy surfaces of BiH_3 calculated for $J = 20$, 40, 60, 80, 100, and 120. The $J = 20$ line is very close to the abscissa and can hardly be seen.

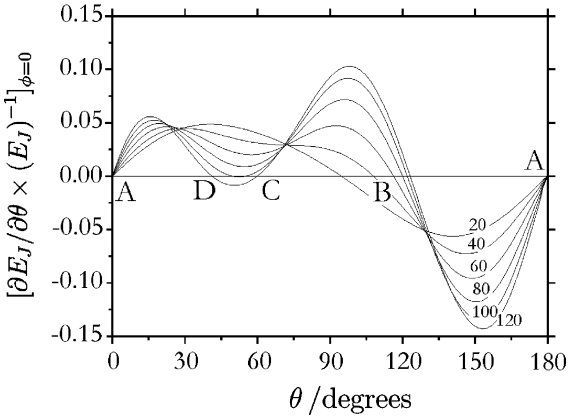

Fig. 9. The function $F_J(\theta) = \partial E_J/\partial\theta \times E_J^{-1}|_{\phi=0}$ for BiH_3 (see text).

dissociated and no stationary geometries can be determined. To identify more clearly the stationary points on the BiH_3 RES, we plot in Fig. 9 the function

$$F_J(\theta) = \left.\frac{\partial E_J}{\partial\theta}\frac{1}{E_J}\right|_{\phi=0} \tag{17}$$

for $J = 20$, 40, 60, 80, 100, and 120, respectively.[2] At each stationary point, we have $F_J(\theta) = 0$, and at these points we further calculate the determinant of the Hessian matrix

$$D = \begin{vmatrix} \frac{\partial^2 E_J}{\partial\theta^2} & \frac{\partial^2 E_J}{\partial\theta\partial\phi} \\ \frac{\partial^2 E_J}{\partial\theta\partial\phi} & \frac{\partial^2 E_J}{\partial\phi^2} \end{vmatrix}. \tag{18}$$

This quantity characterizes stability of the stationary rotational axes and describes the precessional motion of the molecule in their vicinity: $D > 0$ for minima and

[2] The function $F_J(\theta)$ is introduced to identify the points with $\partial E_J/\partial\theta = 0$. The division by E_J is a 'normalization' made so that $F_J(\theta)$ functions with a wide range of J values can be conveniently plotted in the same diagram.

maxima and $D < 0$ for a saddle point. If $D = 0$, tests involving third- and higher-order derivatives must be used to determine the nature of the stationary point.

Each function $F_J(\theta)$ in Fig. 9 has nodes at $\theta = 0°$ and $\theta = 180°$; these nodes are labeled 'A' in the figure. Also, each function has one node (labeled 'B' in the figure) in the interval $90° < \theta < 180°$. The low-J functions have these three nodes only, but as J increases, two additional nodes ('C' and 'D') appear in the interval $0° < \theta < 90°$. The latter two nodes are associated with the fact that for $J > 40$ the one-dimensional cuts in Fig. 8 develop a second maximum around $\theta \approx 35°$ and this maximum must necessarily be accompanied by a minimum separating it from the ever-present maximum at $\theta \approx 120°$. The determinant of the Hessian matrix is zero for the A points in Fig. 9, positive for B and C, and negative for D. The saddle point D separates the localization regions around the points A and C.

The emergence of the two 'new' stationary points C and D at $J \approx 40$ in Fig. 9 represents a process customarily known as a 'bifurcation.' We illustrate this further in the so-called 'bifurcation diagram' of Fig. 10. The diagram shows, as functions of J, the θ values of the B points as a solid line, and those of the points C and D as a dashed line. The dotted line gives the θ values for a set of points at which the determinant of the Hessian matrix is found to vanish. These points suddenly appear at $J \approx 20$ and constitute a 'separatrix' giving rise to the local rotational equilibria C and D at $J \approx 40$ through a so-called 'imperfect bifurcation' [30]. The imperfect bifurcation is evident here because of the characteristic 'pitchfork' signature in Fig. 10 (cf. Fig. 9 of Ref. [31]).

As already mentioned, the points C and D were not encountered in our analysis of the cluster formation in PH_3 [1] and so they are especially interesting. They are obviously formed in a bifurcation process. The stable axis corresponding to point C has $\theta \approx 65°$ at $J = 60$. The optimized geometry for this local rotational equilibrium has all bond lengths approximately equal and angles significantly changed relative to the geometry obtained for the Type B clusters above: $\alpha_2 = \alpha_3$ are increased and α_1 is decreased. At high J, the unstable point D ($\theta \approx 35°$) can be associated with classical rotation about an axis bisecting the H_2BiH_3 angle. During this rotation, centrifugal distortion has the largest effect on the Bi–H_1 bond and the angles α_2 and α_3, while r_2, r_3, and α_1 undergo smaller changes.

The classical trajectories on the RES are closely related to the quantum-mechanical energy values [1,6]. The correlation is very simple—since the energy is necessarily conserved, the trajectory arises as the intersection of the RES with an 'equi-energetic' surface of the given energy, and this surface is a sphere when the RES is presented as a radial plot [6]. Thus, for each of the BiH_3 energy clusters shown in Fig. 2, we can easily find the corresponding classical trajectory: The twofold clusters (Type A) correspond to trajectories around stationary points A with $\theta = 0°$ and $\theta = 180°$. The sixfold clusters of Type B found in the top-right part of Fig. 2 correspond to trajectories circumscribing the maxima on the RES, i.e., the stationary points B. The additional clusters of Type C found at $J > 50$ correspond to trajectories encircling the six minima on the RES, that is, the stationary points C. When this correspondence is established we can also compare, for each cluster type, the average geometries derived from the quantum-mechanical cluster wavefunctions with the geometries obtained from the classical analysis. The former are obtained as quantum-mechanical expectation values of r_i and α_i [1], while the latter are the optimized geometries from the minimization of the classical vibration–rotation energy $E_J(r_i, \alpha_i, \theta, \phi)$. As in the case of PH_3 [1], we have found very good agreement between the 'classical' and 'quantum-mechanical' geometries.

5.2. Semi-classical analysis: θ_k-values

The rotational energy surfaces introduced above give a classical picture of the molecular rotation in the vibrational ground state of a molecule. In order to determine a RES for a vibrationally excited state, special considerations are

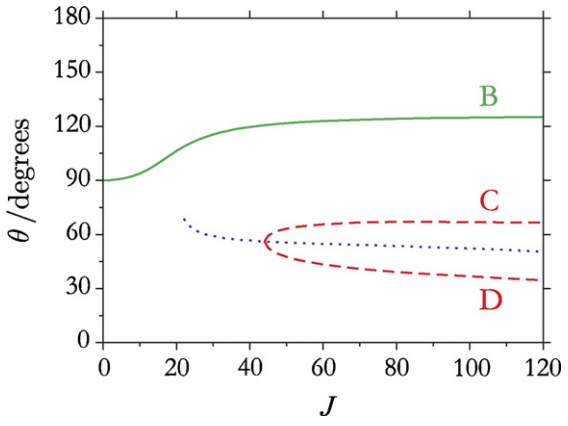

Fig. 10. Values of the polar angle θ for stationary points on the RES's of BiH_3 obtained at different J-values.

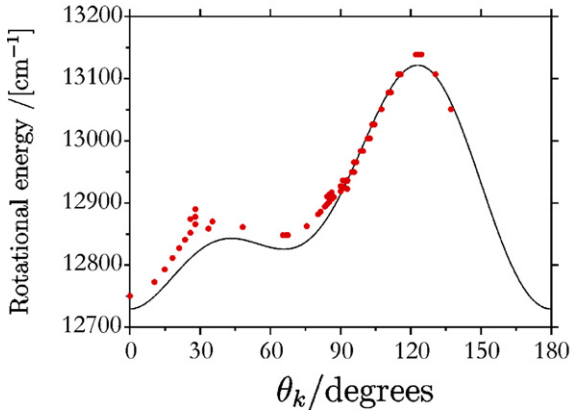

Fig. 11. Energy points (θ_k, $E_{v,Jk}$) (filled circles) and classical rotational energy as a function of θ_k (solid curve) for the vibrational ground state of BiH_3 at $J = 60$ (see text).

necessary [16]. We employ here a semi-classical approach to obtain a RES for excited vibrational states of BiH_3.

The so-called k-probability [27,32] was found to be very useful for identifying the localized rotation axes. In Refs. [27,32], the molecule-fixed axis system was rotated until the z-axis of the rotated axis system coincided with the localized rotation axis; this coincidence manifested itself in an optimally 'sharp' k-distribution with one k-value (normally $k = +J$ or $-J$) having a probability close to unity. In the present work, we do not make such rotations of the molecule-fixed axis system. In our model [14] the K-value measures the projection of the angular momentum onto the molecule-fixed z axis (see Fig. 1), *not* the projection onto the rotation axis A. The quantity $K_{\rm lc}$ is determined quantum-mechanically as the K-value of the basis function $\phi_{v,K}^{J,m}$ with the largest contribution to the eigenfunction $\psi_n^{J,\Gamma}$ (see Eq. (11) and the associated discussion). As discussed previously [1], for the clusters at highest energy in the J manifolds the projection of the angular momentum onto the localized rotation axis A is $J\hbar \approx \sqrt{J(J+1)}\hbar$ for J large. Consequently, we have approximately [1]

$$K_{\rm lc}\hbar = J\hbar|\cos(\theta_k)| = \sqrt{J(J+1)}\hbar|\cos(\theta_k)|, \tag{19}$$

where θ_k is the angle between the z axis and the localized axis of rotation A. Since $K_{\rm lc}$ is the absolute value of the projection of the angular momentum onto the z axis, we cannot determine the sign of $\cos(\theta_k)$. From Eq. (19) (see also Harter [5]), we derive

$$\theta_k = \arccos\left(\frac{\pm K_{\rm lc}}{\sqrt{J(J+1)}}\right). \tag{20}$$

In the classical limit, θ_k defines the orientation of the classical rotation axis relative to the z axis; this angle is identical to the angle θ introduced in Section 5.1. Each eigenfunction $\psi_n^{J\Gamma}$ can be associated with the rotation axis defined by θ_k; this angle is obtained 'semi-classically' since Eq. (20) is derived by classical considerations while the

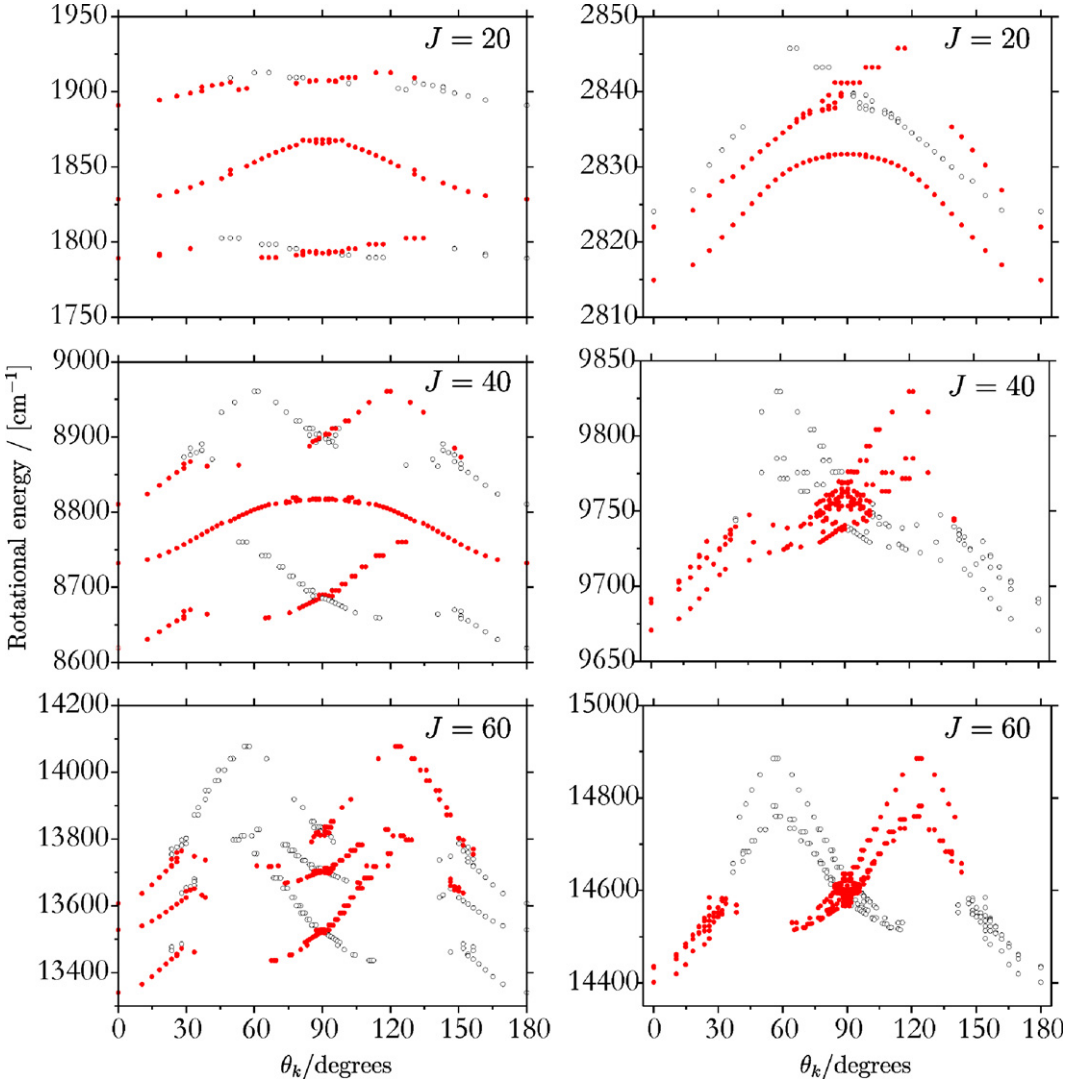

Fig. 12. Energy points (θ_k, $E_{v,Jk}$) for the ν_2/ν_4 (left) and ν_1/ν_3 (right) dyads of BiH_3 (see text).

quantity $K_{\rm lc}$ in Eq. (20) is determined from the quantum-mechanical solution of the rotation–vibration Schrödinger equation. It should be noted, however, that in determining θ_k, we have to choose between $+K_{\rm lc}$ and $-K_{\rm lc}$ in Eq. (20). That is, we have to guess whether a given term value $E_{v,JK_{\rm lc}}$ corresponds to the 'northern' ($\theta_k < 90°$) or 'southern' ($\theta_k > 90°$) rotational hemisphere. Guided by the RES in Fig. 8, we have assumed that all term values $E_{v,Jk}$, which are below the $K_{\rm lc} = 0$ 'separation' region in Fig. 2, have $\theta_k < 90°$ while all term values above the $K_{\rm lc} = 0$ region have $\theta_k > 90°$. This rule follows from the discussion above where we showed that the stationary axes B and C always point into opposite θ-hemispheres.

In Fig. 11, we plot the data points (θ_k, $E_{v,Jk}$), with θ_k calculated from Eq. (20) and $E_{v,Jk}$ computed quantum-mechanically, for $J = 60$. For comparison, we repeat in the figure the one-dimensional RES cut for $J = 60$ from Fig. 8; it is the classical analogue of the semi-classical distribution (θ_k, $E_{v,Jk}$). It is reassuring that the classical curve very closely follows the semi-classical energy points. Thus, with the calculated θ_k-values we can 'reconstruct' a one-dimensional cut through the RES for $\phi = 0°$. We utilize this fact for the analysis of the excited vibrational states.

Fig. 12 presents the (θ_k, $E_{v,Jk}$) distributions for the ν_2/ν_4 and ν_1/ν_3 dyads of BiH_3 (Fig. 2). Now it is no longer straightforward to separate the term values between the two θ-hemispheres because of the overlap of the three components in the dyad. Therefore we initially put all the energies into both hemispheres (empty circles in Fig. 12) and, after a visual inspection of the resulting diagram, we indicate possible distributions by filled circles.

We first comment on the results for the bending fundamental states ν_2/ν_4. We know that sixfold clusters of Type B correspond to maxima, while clusters of Type C correspond to minima on the RES. As we see in the left displays of Fig. 12 the upper progression of points (which is the upper component of the ν_4 state) and the lower progression (the ν_2 state) exhibit maxima at any non-zero J-value. As J increases, the middle progression (i.e., the lower component of the ν_4 state) does not develop such extrema until around $J = 50$ (the maximum at $\theta = 90°$ is an artefact of having put all energies into both θ-hemispheres and does not correspond to sixfold cluster formation). The lower progression eventually joins the middle progression, which means that the clusters of Type B are shared by the ν_2 and ν_4 states. Thus, these clusters are analogous to the Type II clusters characterized by Kozin and Jensen for the ν_1/ν_3 manifolds of H_2Se [27]. At $J = 60$ all progressions in the left display of Fig. 12 have maxima and minima, which suggests that the corresponding term value diagram in Fig. 5 must contain clusters of Types B and C in all three components of the ν_2/ν_4 dyad. However, the term value diagram is so dense in this region that the different cluster types cannot be distinguished with certainty.

The interpretation of the ν_1/ν_3 displays in Fig. 12 is rather straightforward after we have learned how to analyze semi-classical energy distributions. Already at low J, the upper component of the ν_1/ν_3 system develops a one-maximum distribution, indicative of sixfold (Type B) cluster formation. The resulting clusters are shown in Fig. 5. The lower component is featureless at $J = 20$, but by $J = 40$ it exhibits a pronounced maximum (so that Type B clusters are formed) and a shallow minimum (so that Type C clusters are formed). The ν_1/ν_3 display for $J = 60$ shows two very similar profiles, each one resembling that in Fig. 8.

The semi-classical analogues of RES's shown in Fig. 12 provide sketchy outlines of the classical RES's for the vibrationally excited states considered. At very high J values, when the clusters form, the RES's for excited states are similar to the RES of the ground vibration state, in terms of the characteristic stationary points. Obviously, the vibrational excitations are accompanied by interactions between energetically close-lying RES's.

6. Summary and conclusion

Nowadays, energy clustering in XH_N molecules is a well-established and well-studied phenomenon. However, as mentioned above, the work has focused almost exclusively on asymmetric tops XH_2 and spherical tops XH_4. There has been little information available on the symmetric tops XH_3. In our recent theoretical work on PH_3 [1,2] we have tried to remedy this situation. In Ref. [1], we predicted the formation of sixfold near-degenerate energy clusters in the vibrational ground state of PH_3, and in Ref. [2] we calculated the line strengths of the transitions involving the cluster states. In the present work, we have extended the characterization of the cluster formation to the molecules BiH_3 and SbH_3. These molecules are closer to the local-mode limit [10,11] than PH_3 and so the energy clusters form at lower J-values than in PH_3; this means that the calculation of the corresponding energies and wavefunctions require less computational effort than the PH_3 calculations. In consequence, while for PH_3 [1,2] we have described the rotational energy level structure in the vibrational ground state only, for BiH_3 and SbH_3 we have been able to analyze the cluster formation also in excited vibrational states.

The mechanism causing the energy cluster formation in XH_3 molecules is in principle the same, or at least very similar to that responsible for the clustering of energies in XH_2 and XH_4 molecules. Thus, the sixfold energy clusters in PH_3 and SbH_3 come about by a bifurcation effect at a critical J value, just as the fourfold clusters in XH_2 molecules. For BiH_3, the bifurcation is present for all $J > 0$. For all XH_3 molecules considered, the bifurcation process is accompanied by a centrifugal-force-induced dynamical symmetry breaking; analogous effects are found for XH_2 and XH_4 systems. In the case of the quasi-spherical top BiH_3, we have characterized a 'new' type of sixfold clusters, called Type C here, which are related to a so-called imperfect bifurcation. A similar phenomenon has been described in connection with symmetry breaking in quasi-spherical top XY_4 molecules [31].

We have employed a new, semi-classical technique to construct the RES for vibrationally excited states: The K_{lc}-values and the rotational term values obtained in the quantum-mechanical calculations are used in conjunction with the inherently classical Eq. (20). In obtaining the classical RES for the vibrational ground state, we also use a new approach in that we optimize the geometry (by minimizing the energy) at each considered direction of the classical angular momentum (given by θ_m and ϕ_m).

An important aim of the present paper, and of Refs. [1,2], is to inspire spectroscopic experiments with the purpose of observing cluster states in symmetric tops XH_3. That is, we are hoping for a repetition of the XH_2 'story' where the so-called Type I clusters [9] were experimentally observed by Kozin et al. [33] in H_2Se after having been predicted theoretically by Zhilinskií and Pavlichenkov [34], and the Type II clusters [9] were observed in H_2Se by Flaud et al. [35] after having been independently predicted by Lehmann [36,37] and by Kozin and Jensen [27]. It seems to us that the most promising way of characterizing experimentally the cluster levels in the vibrational ground states of XH_3 molecules is to observe the so-called intra-cluster transitions [2]; these transitions take place between states within the same cluster. As J increases, the corresponding transition wavenumbers move through the THz, mm-wave, and microwave regions where ultra-high-resolution and ultra-high-sensitivity spectroscopy is possible. We are well aware, however, of the substantial challenges associated with experiments of this type on the XH_3 molecules that we have investigated theoretically. The transitions involving the cluster states are very weak as they start in highly excited rotational states. Furthermore, PH_3 is poisonous and BiH_3 rapidly decomposes at temperatures above −40 °C [38]. Even though our calculations indicate that in BiH_3, the clusters form at lower J values than in PH_3 and SbH_3, so that BiH_3 would seem to be the most promising candidate for the observation of cluster transitions, its instability precludes a heating of the sample which could help populate the initial states of the intra-cluster transitions. Also, the synthesis of BiH_3 is difficult [13,38]. It remains to be seen whether these obstacles can be overcome in future experimental studies.

Acknowledgments

The work of P.J. is supported in part by the Fonds der Chemischen Industrie. We acknowledge support from the European Commission through Contract No. MRTN-CT-2004-512202 "Quantitative Spectroscopy for Atmospheric and Astrophysical Research" (QUASAAR). We thank Jon T. Hougen for helpful comments on the cluster splittings and S. Petrov for his interest and for drawing our attention to the imperfect bifurcation process.

References

[1] S.N. Yurchenko, W. Thiel, S. Patchkovskii, P. Jensen, Phys. Chem. Chem. Phys. 7 (2005) 573–582.
[2] S.N. Yurchenko, M. Carvajal, W. Thiel, P. Jensen, J. Mol. Spectrosc. 239 (2006) 71–87.
[3] P.R. Bunker, P. Jensen, Molecular Symmetry and Spectroscopy, second ed., NRC Research Press, Ottawa, 1998.
[4] A.J. Dorney, J.K.G. Watson, J. Mol. Spectrosc. 42 (1972) 135–148.
[5] W.G. Harter, C.W. Patterson, J. Chem. Phys. 80 (1984) 4241–4261.
[6] W.G. Harter, Comp. Phys. Rep. 8 (1988) 319–394.
[7] I.M. Pavlichenkov, B.I. Zhilinskií, Ann. Phys. 184 (1988) 1–32.
[8] K. Efstathiou, D.A. Sadovskií, B.I. Zhilinskií, SIAM J. Appl. Dyn. Sys. 3 (2004) 261–351.
[9] P. Jensen, G. Osmann, I.N. Kozin, in: D. Papoušek (Ed.), Vibration–Rotational Spectroscopy and Molecular Dynamics, World Scientific, Singapore, 1997.
[10] P. Jensen, Mol. Phys. 98 (2000) 1253–1285.
[11] L. Halonen, A.G. Robiette, J. Chem. Phys 84 (1986) 6861–6871.
[12] W. Jerzembeck, H. Bürger, V. Hänninen, L. Halonen, J. Chem. Phys. 120 (2004) 5650–5656.
[13] W. Jerzembeck, H. Bürger, L. Constantin, L. Margulès, J. Demaison, J. Breidung, W. Thiel, Angew. Chem., Int. Ed. Engl. 41 (2002) 2550–2552.
[14] S.N. Yurchenko, M. Carvajal, P. Jensen, H. Lin, J.J. Zheng, W. Thiel, Mol. Phys. 103 (2005) 359–378.
[15] D.A. Sadovskií, B.I. Zhilinskií, Mol. Phys. 65 (1988) 109–128.
[16] Ch. van Hecke, D.A. Sadovskií, B.I. Zhilinskií, V. Boudon, Eur. Phys. J. D 17 (2001) 13–35.
[17] S.N. Yurchenko, J. Breidung, W. Thiel, Theor. Chem. Acc. 114 (2005) 333–340.
[18] E. Canè, G. Di Lonardo, L. Fusina, W. Jerzembeck, H. Bürger, J. Breidung, W. Thiel, Mol. Phys. 103 (2005) 557–577.
[19] W. Jerzembeck, H. Bürger, J. Breidung, W. Thiel, J. Mol. Spectrosc. 226 (2004) 32–44.
[20] H. Harder, C. Gerke, L. Fusina, J. Chem. Phys. 114 (2001) 3508–3523.
[21] S.N. Yurchenko, M. Carvajal, W. Thiel, H. Lin, P. Jensen, Adv. Quant. Chem. 48 (2005) 209–238.
[22] S.N. Yurchenko, M. Carvajal, H. Lin, J.J. Zheng, W. Thiel, P. Jensen, J. Chem. Phys. 122 (2005) 104317.
[23] J.T. Hougen, P.R. Bunker, J.W.C. Johns, J. Mol. Spectrosc. 34 (1970) 136–172.
[24] C. Eckart, Phys. Rev. 47 (1935) 552–558.
[25] A. Sayvetz, J. Chem. Phys. 7 (1939) 383–389.
[26] D.A. Sadovskií, B.I. Zhilinskií, J.P. Champion, G. Pierre, J. Chem. Phys. 92 (1990) 1523–1537.
[27] I.N. Kozin, P. Jensen, J. Mol. Spectrosc. 161 (1993) 186–207.
[28] I.N. Kozin, I.M. Pavlichenkov, J. Chem. Phys. 104 (1996) 4105–4113.
[29] J.A. Montaldi, R.M. Roberts, J. Nonlinear Sci. 9 (1999) 53–88.
[30] M. Golubitsky, D.G. Schaeffer, Singularities and Groups in Bifurcation Theory, vol. 1, Springer-Verlag, Berlin, 1984.
[31] B.I. Zhilinskií, I.N. Kozin, S. Petrov, Spectrochim. Acta A 55 (1999) 1471–1484.
[32] S.G. Larsen, S. Brodersen, J. Mol. Spectrosc. 157 (1993) 220–236.
[33] I.N. Kozin, S.P. Belov, O.L. Polyanski, M. Yu. Tretyakov, J. Mol. Spectrosc. 152 (1992) 13–28.
[34] B.I. Zhilinskii, I.M. Pavlichenkov, Opt. Spectrosc. (USSR) 64 (1988) 413–414.
[35] J.-M. Flaud, C. Camy-Peyret, H. Bürger, P. Jensen, I.N. Kozin, J. Mol. Spectrosc. 172 (1995) 126–134.
[36] K.K. Lehmann, J. Chem. Phys. 95 (1991) 2361–2370.
[37] K.K. Lehmann, J. Chem. Phys. 96 (1992) 7402–7409.
[38] E. Amberger, Chem. Ber. 94 (1961) 1447–1452.